Impact of Finite-Temperature and Condensed-Phase Effects on Theoretical X-Ray Absorption Spectra of Transition Metal Complexes

Patrick Müller,[a] Kristof Karhan,[a] Matthias Krack,[b] Uwe Gerstmann,[c] Wolf Gero Schmidt,[c] Matthias Bauer,[d] and Thomas D. Kühne *[d]

The impact of condensed-phase and finite-temperature effects on the theoretical X-ray absorption spectra of transition metal complexes is assessed. The former are included in terms of the all-electron Gaussian and augmented plane-wave approach, whereas the latter are taken into account by extensive ensemble averaging along second-generation Car–Parrinello ab initio molecular dynamics trajectories. We find that employing the periodic boundary conditions and including finite-temperature effects systematically improves the agreement between our simulated X-ray absorption spectra and experimental measurements. © 2018 Wiley Periodicals, Inc.

DOI:10.1002/jcc.25641

Introduction

X-ray absorption spectroscopy (XAS) at transition metal K-edges has proven to be a powerful tool to investigate the working principle of transition metal centers in catalysts, functional materials, and enzymes over the last decades.[1–6] The method's success is because of the fact that it provides both information on the electronic details and local structure of the functional metal center, being fully independent of the state of aggregation.[7] In a typical XAS experiment, the attenuation of an incoming X-ray beam by absorption through a sample is measured as a function of energy. The corresponding X-ray absorption spectrum is obtained by applying Lambert–Beers law. It is characterized by a sharp edge-step caused by a resonant excitation of a 1*s* electron in case of so-called K-edge spectra, which are the subject of this work. Although no sharp separation exists, the interval from around 15 eV before the edge till 40 eV thereafter is called the X-ray absorption near edge structure (XANES) region including pre-edge signals, while the region starting from 40 eV above the edge is defined as the extended X-ray absorption fine structure (EXAFS) region, which is indicated in Figure 1.

Typically, in the XANES part, the so-called prepeak, caused by $1s \rightarrow nd$ transitions, is used to obtain information about the lowest unoccupied molecular orbital (LUMO) states by application of density functional theory (DFT) methods.[8–10] The absorption edge itself and the following intense first oscillations are mostly treated in a comparative way using highly defined references to extract oxidation states and a rough estimation of the local structure.[11] The latter one is then achieved by analysis of the oscillations in the EXAFS part, including type, number, and distances of coordinating ligand atoms.[7,12,13]

Although this three step analysis approach is highly valuable and frequently used, it neglects the superior potential of the XANES region, as it carries basically the full information about the geometric (backscattering) and electronic (orbital contributions) situation. This advantage becomes even larger if the much better signal to noise ratio of XANES spectra compared to EXAFS spectra is taken into account.

Making full use of the information content in K-edge XANES data is limited by the lifetime broadening of the 1*s* electron hole after K-edge excitation.[14] This broadening limits the extraction of information from the pre-edge peak and XANES region significantly, as details of the spectroscopic signatures are smeared out.[14–16] Consequently, the value of comparing such lifetime broadened spectra to highly precise theoretical calculations is limited.

To make use of XANES spectra to the largest possible extent, two main conditions have to be met:

[a] *P. Müller, K. Karhan*
Department of Chemistry, University of Paderborn, Warburger Str. 100, 33098, Paderborn, Germany
[b] *M. Krack*
Laboratory for Scientific Computing and Modelling, Paul Scherrer Institut, CH-5232, Villigen PSI, Switzerland
[c] *U. Gerstmann, W. Gero Schmidt*
Department of Physics, University of Paderborn, Warburger Str. 100, 33098, Paderborn, Germany
[d] *M. Bauer, T. D. Kühne*
Department of Chemistry and Center for Sustainable Systems Design, University of Paderborn, Warburger Str. 100, 33098, Paderborn, Germany
E-mail: tdkuehne@mail.upb.de

This project has received funding from the European Research Council (ERC) under the European Union's Horizon 2020 research and innovation programme (grant agreement no. 716142). M.B., P.M., W.G.S., and U.G. received funding from the Forschergruppe 1405 of the German Research Council. M.B. received funding from the German Ministry for Science and Education in frame of project SusChEmX (FKZ 05K14PP1).
Contract Grant sponsor: Bundesministerium für Bildung und Forschung; Contract Grant number: SusChEmX (FKZ 05K14PP1); Contract Grant sponsor: H2020 European Research Council; Contract Grant number: grant agreement No 716142; Contract Grant sponsor: German Ministry for Science and Education; Contract Grant number: FKZ 05K14PP1; Contract Grant sponsor: German Research Council; Contract Grant sponsor: European Research Council (ERC); Contract Grant number: 716142

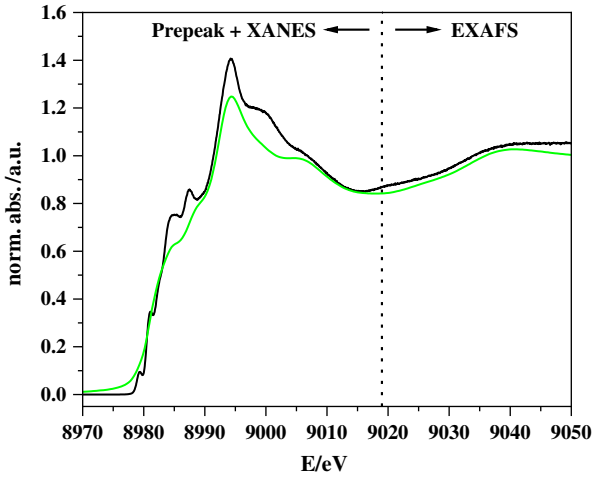

Figure 1. Comparison of the conventional (green) and high energy resolution XANES spectra (black) of $[Cu(I)(DMEGqu)_2](PF_6)$. The effect of the high resolution detection mode is particularly visible in the XANES region. [Color figure can be viewed at wileyonlinelibrary.com]

1. The lifetime broadening of K-edge XANES data needs to be reduced.
2. An accurate theoretical description of the prepeak and XANES feature has to be achieved over the full XANES energy range.

With the advent of high resolution partial fluorescence yield detection using Johann-type spectrometers,[17] high energy resolution fluorescence detected XANES (HERFD-XANES) spectra can be obtained.[14] HERFD-XANES spectra are recorded by monitoring the intensity of a narrow emission line range in such a way that the lifetime broadening of K-edge spectra is nearly eliminated. However, it still has to be taken into account that an experimental broadening from the beamline and spectrometer is present.[15] Overall, a reduction from around 5–1.5 eV in first row transition metal K-edges can be achieved, and condition 1 is met. The effect of high resolution fluorescence detection is demonstrated in Figure 1 for the example of the biomimetic Cu(I) complex formed by the quinoline-based ligand N-(1,3-dimethyl-imidazolidin-2-ylidene)quinolin-8-amine (DMEGqu), that is, $[Cu(I)(DMEGqu)_2](PF_6)$, by comparing the conventional with high resolution spectra.[18,19]

As the geometric and electronic structure plays a central role for the electron transfer efficiency of such copper complexes, their investigation using XAS and theoretical techniques can therefore significantly contribute to the understanding of copper mediated electron transfer processes in general. However, with condition 2, several issues are connected. The application of pseudopotential methods to treat core-hole excitations is not straightforward. On the other hand, all-electron calculations are particularly more suited for describing X-ray absorption, but come with the disadvantage of larger computational costs.[20]

Although Kohn–Sham (KS) DFT is commonly used to describe complex structures, especially the description of excited states is more precisely treated by for example the so-called GW approximation for the electronic self-energies and the Bethe–Salpeter approach to describe Coulomb coupled electron–hole pairs.[21,22] Time-dependent DFT (TD-DFT) is currently the method of choice to address charge neutral excitations and to determine core excitations,[23–26] but on the price of the unknown TD exchange and correlation (XC) potential. Most numerical implementations rely on the adiabatic approximation, which often proves successful for finite systems such as molecules, but fails for extended systems such as solids.

Also critical for the simulation of X-ray absorption spectra is the basis set used to expand the electronic wave function. On the one hand, localized basis functions are computationally efficient and thus allow for the modeling of core electrons as well as many-body effects. However, even though systematically improvable, they do not form a complete set and are not suitable for the description of excited delocalized high-energy states. Plane waves, on the other hand, form by construction an orthogonal basis set that can be trivially improved by varying the corresponding cutoff energy. Moreover, plane waves are ideally suited to describe delocalized high-energy states as well as systems with periodic boundary conditions such as molecular crystals. Naturally, the description of core states with plane waves is cumbersome.

Although most of the developments for the simulation of XANES spectra focused on the improved description of the electronic structure of the material under investigation, temperature effects, the systems dynamics, and environmental or matrix factors are rarely in the center of interest. Hence, in this work, we assess the impact of finite-temperature and condensed-phase effects on theoretical X-ray absorption spectra of complex systems in the gas and liquid phase, as well as in water solution.

The remaining of this article is organized as follows. "Methodology and computational details" section describes the employed methods to compute X-ray absorption spectra (XAS) within the all-electron Gaussian and augmented plane-wave (GAPW) approach, as well as the computational details. Further explanation and interpretation of results are discussed in "Results and discussion" section followed by "Conclusions" section.

Methodology and Computational Details

In particular, we are comparing the computed XAS spectra of the aforementioned Cu(I) complex in the gas (69 atoms) and in the crystalline phase (76 atoms), with that of a single complex in water solution (432 atoms), all at 0 K and 300 K. All calculations were conducted at the DFT level using the CP2K suite of programs,[27] where the exact XC functional is substituted by the Becke–Lee–Yang–Parr generalized gradient approximation.[28,29] The atomic configurations were obtained using the mixed Gaussian and plane-wave approach in conjunction with separable and norm-conserving pseudopotentials to describe the interactions between the valence electrons and the ionic cores.[30–32] In this approach, the KS orbitals are expanded in Gaussians, while for the electron density a plane-wave basis is employed. The former are represented by an accurate molecularly optimized double-ζ basis set with one set of polarization functions (DZVP),[33] while a density cutoff of 360 Ry is used for

the charge density. For the purpose to compute the static XAS spectra, the nuclear ground-state at 0 K is located by minimizing the total energy with the limited-memory Broyden–Fletcher–Goldfarb–Shanno algorithm.[34] To mimic an extended condensed-phase system, 3D periodic boundary condition were employed, while, in the gas phase, the Poisson problem is tackled using an efficient wavelet-based solver and a vacuum portion of 6 Å along all three nonperiodic directions.[35] In order to assess the impact of finite-temperature effects, DFT-based ab initio molecular dynamics (AIMD) simulations were performed using the second generation Car–Parrinello approach of Kühne et al.[36–39] For each system we are considering here, the modified Langevin equation is integrated for 25 ps to equilibrate the system followed by additional 100 ps in order to accumulate statistics, all using a discretized time-step of 0.5 fs. Out of these trajectories, the eventual finite-temperature XAS spectra are each computed as ensemble averages over 50 statistical independent configurations that are separated by 2 ps.

The XAS spectra were simulated at the copper K-edge using the full-core-hole (FCH) transition potential formalism,[40–42] as implemented in the all-electron GAPW approach.[43–45] As before, the GAPW method consists of a dual basis set made up of localized Gaussian type orbitals to describe the KS orbitals, as well as plane waves to represent only the smoothly varying density between the atoms.[46,47] For the latter, a density cutoff of 480 Ry is employed, whereas the all-electron orbitals are described by consistent DZVP Gaussian basis set for solid-state calculations of Bredow and coworkers.[48]

Because of the fact that the energy functional depends parametrically on the occupation number of the KS orbitals,[49] the transition energies can be determined by computing the total energy differences between the ground and an excited state that is obtained by promoting an electron into a virtual orbital. Both, the initial and final states can be directly approximated by selected orbitals that are solutions of the KS equations with a modified core-hole potential on the absorbing atom. Because we assume that the location of the promoted electron is immediately delocalized in the conduction band, its contribution to the final spectrum is essentially independent of the final state, which allows computing the whole spectrum with just one electronic structure calculation. In the single electron picture, the transition probabilities simplifies to dipole transition elements between the initial and final orbitals. Thus, $I \propto |\langle \psi'_f | \mathbf{E}\mu | \psi'_{\mathrm{core}} \rangle|^2$, where $\mathbf{E}$ is the electric field representing the incoming photon and μ is the dipole operator. Yet, in the case of soft X-rays, where the wavelength of the interacting photon is much larger than the molecular dimension, it suffices to consider just the first term in the expansion of the electric field. In this so-called electric dipole approximation, the transition probabilities are proportional to the orbital-dipole integral along the polarization direction l, that is, $|\langle \psi'_f | \mathbf{r}_l | \psi'_{\mathrm{core}} \rangle|^2$. For the purpose to uniquely associate the core orbitals to the atomic centers, the canonical orbitals are substituted by maximally localized Wannier functions as obtained the scheme of Berghold et al.[50] The localized core orbital ψ^A_{core} are characterized by maximizing the overlap between ψ^A_{core} and the functions of a minimal Slater-type basis set STO^A_α with respect to α, which denotes the energy level and angular momentum. By changing the occupation number of the excited core-hole orbital, the selected core-hole potential is applied that is followed by a variational optimization of the modified KS equations within the local spin density approximation to accommodate for the spin polarization because of removing an electron from the core. While, as already alluded to above, the dynamic XAS spectra at finite-temperature are computed as an ensemble average, in the static case, the eventual discrete spectral distribution, which is determined in terms of transition moment integrals in the velocity form, are convoluted by Gaussian functions to mimic the experimental broadening. Specifically, for all static spectra a constant Gaussian width of 0.5 eV is used below the edge, followed by a linearly increasing width up to 8 eV over the following 20 eV.[51]

HERFD-XANES experiments were performed at beamline ID26 of the European Synchrotron Radiation Facility (ESRF) in Grenoble (France). For the measurements at the copper K-edge (8979 eV), a Si(311) double-crystal monochromator was used. The maximum beam current was 200 mA with a ring-energy of 6 GeV. For the K-edge measurements, the solid samples were prepared as wafers using degassed cellulose as a binder to avoid self-absorption effects. The spectra were recorded at 30 K in a closed cycle helium cryostat. The Cu(I) samples were additionally prepared under inert atmosphere in a glove box and spectrometer was kept under helium atmosphere to reduce the absorption of the fluorescence radiation. No signs of radiation damage could be detected in any sample within the acquisition time and measurements were carried out on multiple spots.

Results and Discussion

Blue copper or type-one proteins span a large window of reduction potentials that leads to a variety of possible electron transfer partners.[1,2] However, subject to the present investigation are so-called type-zero biomimetic copper complexes, which exhibit electron transfer features similar to blue copper proteins, but with hard nitrogen instead of sulfur donor ligands.[52] The electron transfer properties of such complexes depend crucially on the structural details at the Cu(I) center,[53–55] which are closely correlated to the electronic properties of the compounds. As a prototype model for type-zero complexes, we use the aforementioned Cu(I) complex formed by the quinoline-based ligand DMEGqu, that is, $[\mathrm{Cu(I)(DMEGqu)_2}](\mathrm{PF_6})$.[18,19] Yet, in order to understand the working principle of biomimetic complexes, it is of course mandatory to access their electronic and structural details in situ, which is a highly demanding task that is perfectly matched by XANES spectroscopy. However, the sensitivity of XANES toward temperature effects, cluster sizes, and solvent influences is rarely addressed.

In general, the spectrum can roughly be divided into two sections. The first one being transitions into discrete orbitals with and without charge transfer character in the region up to 8985 eV and transitions into the continuum after that. As can be seen in Figure 2, the computed spectrum of using a single Cu(I) complex in the gas phase, whose structure has been

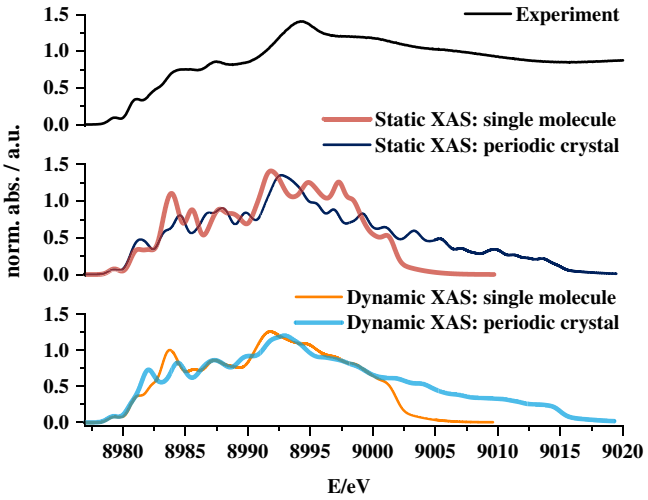

Figure 2. Experimental and simulated XAS spectra of the Cu(I) complex as obtained by static (0 K) and dynamic (300 K) calculations in the gas (single molecule), as well as condensed-phase (periodic crystal). [Color figure can be viewed at wileyonlinelibrary.com]

optimized to yield the nuclear ground-state at 0 K, already qualitatively reproduces most experimental features up to 9000 eV. In particular, the energetic position of the transitions is described reasonably well; although, the intensity differs for some of them. For example, the peak at 8984 eV is quite strongly overestimated in its intensity. Furthermore, within the simulated spectra, most of the features are too narrow. Nevertheless, this can be corrected increasing the artificial broadening of the calculated transitions. However, computing the same XAS spectrum at finite-temperature exhibits several differences. In spite of the fact that because of the ensemble averaging, no artificial broadening is necessary, the spectra are throughout much smoother and generally in better agreement with the experimental reference. Still, the intensity of the peak at 8984 eV is overestimated and the white line at 8994 eV is shifted to a lower energy of 8992 eV in the calculation. This is to say that although the intensity of the spectrum is not quantitatively reproduced, the general shape and oscillations as obtained by the combined AIMD-XAS approach are in qualitative good agreement with experiment.

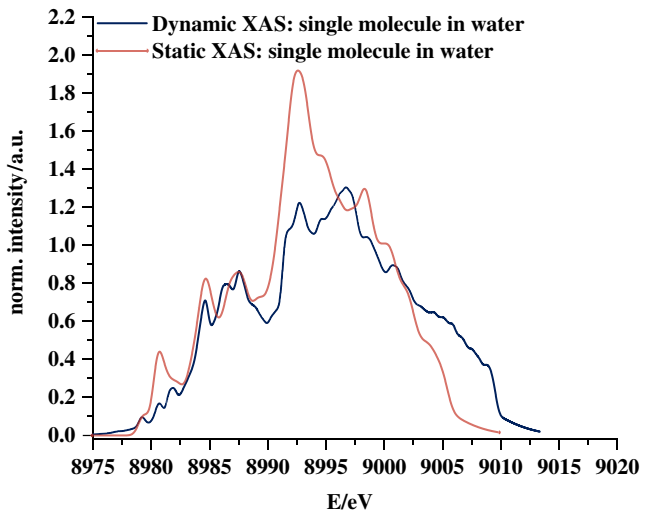

Figure 3. Simulated XAS spectra of a single Cu(I) complex in water solution, as obtained by dynamic (300 K) and static (0 K) condensed-phase calculations using periodic boundary conditions. [Color figure can be viewed at wileyonlinelibrary.com]

Yet, because the experimental spectra are obtained from solid state measurements, additional condensed-phase XAS calculations of the crystal structure using periodic boundary conditions were conducted. Already the static condensed-phase calculation represents a systematic improvement compared with the single molecule calculations. The energetic position and the intensity of the peaks are very well reproduced and the spectral shape is in very good agreement up to the white line. At higher energies, however, the oscillations are too narrow compared to the experimental measurement. Nevertheless, including finite-temperature effects, the latter part of spectrum is again significantly improved and reproduces the experimental curve rather well, but lacks the very good agreement for the second transition at 8982 eV, which is strongly overestimated. Comparing the dynamic finite-temperature simulations with their static counterparts at 0 K, it is apparent that, although the combined AIMD-XAS approach entails a systematically increased agreement with experiment in the high energy part of the spectrum, the improvement is relatively small in particular when considering the much larger computational effort of the AIMD simulations. On that occasion, we find it important to make a note that the investigated Cu(I) complex is rather stiff with a very hydrophobic ligand. This immediately suggests that the XAS response because of conformational fluctuations, which is the chief advantage of the present AIMD-XAS method to take those explicitly into account, is much higher when using other hydrophilic ligands.

In addition, to investigate the effect of solvation on the XAS spectrum, calculations of a single molecule in water solution were conducted for comparison. As can be seen in Figure 3, the most obvious difference in the XAS spectrum between the static and dynamic calculations in water solution is the intensity ratio between the white line and the other transitions. Another distinct difference is the shoulder at 8982 eV, which is absent in the simulated finite-temperature water solution spectrum. Because the underlying transition has some charge transfer character,[19] it might be shifted to higher or lower energies or just be dampened in intensity. Therefore, it might not be visible anymore. Even though the simulated XAS spectra cannot be directly compared to the present experiment because of the difference of solvent, it nevertheless demonstrates the feasibility of this approach to compute XAS spectra of complex molecules in aqueous solution, which is critical for further studies, for example, photocatalytic water splitting. Further mixed computational and experimental studies on complexes in aqueous solution have to be carried out in the future to shed light on these effects, which could either be of electronic or geometric nature.

Conclusions

In conclusion, we have assessed the impact of finite-temperature and condensed-phase effects on theoretical X-ray absorption spectra of transition metal complexes. We found

that the usage of periodic boundary conditions entails a systematic improvement of the simulated XAS spectrum within the EXAFS range, though quantitative agreement with experiment cannot be achieved using a simple single electron approach. Nevertheless, further quantitative improvements can be achieved by the inclusion of finite-temperature effects using the present combined AIMD-XAS scheme.

Acknowledgments

Sonja Herres-Pawlis (RWTH Aachen) is kindly acknowledged for provision of samples and beamline ID26 at the ESRF (Grenoble) for provision of beamtime. The authors would like to thank the Gauss Center for Supercomputing (GCS) for providing computing time through the John von Neumann Institute for Computing (NIC) on the GCS share of the supercomputer JUWELS at the Jülich Supercomputing Centre (JSC) and on the GCS Supercomputer SuperMUC at Leibniz Supercomputing Centre (www.lrz.de). The generous allocation of supercomputing time on OCuLUS at the Paderborn Center for Parallel Computing (PC^2) (https://pc2.uni-paderborn.de/hpc-services/available-systems/oculus/) is knidly acknowledged.

Keywords: ab initio molecular dynamics · Car–Parrinello molecular dynamics · X-ray absorption spectroscopy · X-ray absorption near edge structure · near edge X-ray absorption fine structure

How to cite this article: P. Müller, K. Karhan, M. Krack, U. Gerstmann, W. G. Schmidt, M. Bauer, T. D. Kühne. *J. Comput. Chem.* **2019**, *40*, 712–716. DOI: 10.1002/jcc.25641

[1] L. E. Aleandri, B. Bogdanović, C. Dürr, S. C. Huckett, D. J. Jones, U. Kolb, M. Lagarden, J. Rozière, U. Wilczok, *Chem. A Eur. J.* **1997**, *3*, 1710.
[2] H. Dau, P. Liebisch, M. Haumann, *Anal. Bioanal. Chem.* **2003**, *376*, 562.
[3] M. Haumann, P. Liebisch, C. Müller, M. Barra, M. Grabolle, H. Dau, *Science* **2005**, *310*, 1019.
[4] A. S. K. Hashmi, C. Lothschütz, M. Ackermann, R. Doepp, S. Anantharaman, B. Marchetti, H. Bertagnolli, F. Rominger, *Chem. A Eur. J.* **2010**, *16*, 8012.
[5] P. Glatzel, T. -C. Weng, K. Kvashnina, J. Swarbrick, M. Sikora, E. Gallo, N. Smolentsev, R. A. Mori, *J. Electr. Spectrosc. Relat. Phenom.* **2013**, *188*, 17.
[6] R. Bjornsson, M. U. Delgado-Jaime, F. A. Lima, D. Sippel, J. Schlesier, T. Weyhermüller, O. Einsle, F. Neese, S. de Beer, *Z. Anorg. Allg. Chem.* **2015**, *641*, 65.
[7] M. Bauer, H. Bertagnolli, Methods in Physical Chemistry, Wiley-VCH Verlag GmbH & Co. KGaA, Weinheim, Germany, **2012**, p. 231.
[8] S. DeBeer George, T. Petrenko, F. Neese, *Inorg. Chim. Acta* **2008**, *361*, 965.
[9] P. Chandrasekaran, S. C. E. Stieber, T. J. Collins, L. Que, Jr., F. Neese, S. DeBeer, *Dalton Trans.* **2011**, *40*, 11070.
[10] V. Krewald, B. Lassalle-Kaiser, T. T. Boron, C. J. Pollock, J. Kern, M. A. Beckwith, V. K. Yachandra, V. L. Pecoraro, J. Yano, F. Neese, S. DeBeer, *Inorg. Chem.* **2013**, *52*, 12904.
[11] R. Schoch, W. Desens, T. Werner, M. Bauer, *Chem. A Eur. J.* **2013**, *19*, 15816.
[12] H. Bertagnolli, T. S. Ertel, *Angew. Chem. Int. Ed.* **1994**, *33*, 45.
[13] M. Bauer, C. Gastl, *Phys. Chem. Chem. Phys.* **2010**, *12*, 5575.
[14] P. Glatzel, U. Bergmann, *Coord. Chem. Rev.* **2005**, *249*, 65.
[15] M. Bauer, *Phys. Chem. Chem. Phys.* **2014**, *16*, 13827.
[16] A. J. Atkins, M. Bauer, C. R. Jacob, *Phys. Chem. Chem. Phys.* **2015**, *17*, 13937.
[17] H. H. Johann, *Z. Phys.* **1931**, *69*, 185.
[18] A. Hoffmann, J. Stanek, B. Dicke, L. Peters, B. Grimm-Lebsanft, A. Wetzel, A. Jesser, M. Bauer, M. Gnida, W. Meyer-Klaucke, M. Rübhausen, S. Herres-Pawlis, *Eur. J. Inorg. Chem.* **2016**, *2016*, 4731.
[19] N. J. Vollmers, P. Müller, A. Hoffmann, S. Herres-Pawlis, M. Rohrmüller, W. G. Schmidt, U. Gerstmann, M. Bauer, *Inorg. Chem.* **2016**, *55*, 11694.
[20] L. Triguero, L. G. M. Pettersson, H. Agren, *Phys. Rev. B* **1998**, *58*, 8097.
[21] E. L. Shirley, *Phys. Rev. Lett.* **1998**, *80*, 794.
[22] F. Bechstedt, Many-Body Approach to Electronic Excitations. Springer Series in Solid-State Sciences, Vol. *181*, Springer Berlin Heidelberg, Berlin, Heidelberg, Germany, **2015**.
[23] N. A. Besley, A. T. B. Gilbert, P. M. W. Gill, *J. Chem. Phys.* **2009**, *130*, 124308.
[24] S. DeBeer George, T. Petrenko, F. Neese, *J. Phys. Chem. A* **2008**, *112*, 12936.
[25] Y. Zhang, S. Mukamel, M. Khalil, N. Govind, *J. Chem. Theory Comput.* **2015**, *11*, 5804.
[26] I. P. E. Roper, N. A. Besley, *J. Chem. Phys.* **2016**, *144*, 114104.
[27] J. Vande Vondele, M. Krack, F. Mohamed, M. Parrinello, T. Chassaing, J. Hutter, *Comput. Phys. Commun.* **2005**, *167*, 103.
[28] A. D. Becke, *Phys. Rev. A* **1988**, *38*, 3098.
[29] C. T. Lee, W. T. Yang, R. G. Parr, *Phys. Rev. B* **1988**, *37*, 785.
[30] G. Lippert, J. Hutter, M. Parrinello, *Mol. Phys.* **1997**, *92*, 477.
[31] S. Goedecker, M. Teter, J. Hutter, *Phys. Rev. B* **1996**, *54*, 1703.
[32] M. Krack, *Theor. Chem. Acc.* **2005**, *114*, 145.
[33] J. Vande Vondele, J. Hutter, *J. Chem. Phys.* **2007**, *127*, 114105.
[34] J. Nocedal, *Math. Comput.* **1980**, *35*, 773.
[35] L. Genovese, T. Deutsch, A. Neelov, S. Goedecker, G. Beylkin, *J. Chem. Phys.* **2006**, *125*, 074105.
[36] T. D. Kühne, M. Krack, F. R. Mohamed, M. Parrinello, *Phys. Rev. Lett.* **2007**, *98*.
[37] T. D. Kühne, M. Krack, M. Parrinello, *J. Chem. Theory Comput.* **2009**, *5*, 235.
[38] T. D. Kühne, *WIREs Comput. Mol. Sci.* **2014**, *4*, 391.
[39] T. D. Kühne, E. Prodan, *Ann. Phys. Rehabil. Med.* **2018**, *391*, 120.
[40] B. Hetenyi, F. De Angelis, P. Giannozzi, R. Car, *J. Chem. Phys.* **2004**, *120*, 8632.
[41] M. Cavalleri, M. Odelius, D. Nordlund, A. Nilsson, L. G. M. Pettersson, *Phys. Chem. Chem. Phys.* **2005**, *7*, 2854.
[42] D. Prendergast, G. Galli, *Phys. Rev. Lett.* **2006**, *96*.
[43] M. Iannuzzi, T. Chassaing, T. Wallman, J. Hutter, *CHIMIA* **2005**, *59*, 499.
[44] M. Iannuzzi, J. Hutter, *Phys. Chem. Chem. Phys.* **2007**, *9*, 1599.
[45] M. Iannuzzi, *J. Chem. Phys.* **2008**, *128*, 204506.
[46] G. Lippert, J. Hutter, M. Parrinello, *Theor. Chem. Acc.* **1999**, *103*, 124.
[47] M. Krack, M. Parrinello, *Phys. Chem. Chem. Phys.* **2000**, *2*, 2105.
[48] M. F. Peintinger, D. Vilela Oliveira, T. Bredow, *J. Comput. Chem.* **2012**, *34*, 451.
[49] J. F. Janak, *Phys. Rev. B* **1978**, *18*, 7165.
[50] G. Berghold, C. J. Mundy, A. H. Romero, J. Hutter, M. Parrinello, *Phys. Rev. B* **2000**, *61*, 10,040.
[51] M. Cavalleri, M. Odelius, A. Nilsson, L. Pettersson, *J. Chem. Phys.* **2004**, *121*, 065.
[52] K. M. Lancaster, S. DeBeer George, K. Yokoyama, J. H. Richards, H. B. Gray, *Nat. Chem.* **2009**, *1*, 711.
[53] H. B. Gray, B. G. Malmström, R. J. P. Williams, *J. Biol. Inorg. Chem.* **2000**, *5*, 551.
[54] D. B. Rorabacher, *Chem. Rev.* **2004**, *104*, 651.
[55] P. Comba, M. Kerscher, *Coord. Chem. Rev.* **2009**, *253*, 564.

Received: 23 May 2018
Revised: 20 August 2018
Accepted: 18 September 2018
Published online on 11 October 2018